# Accurate Monte Carlo modeling and performance assessment of the X-PET™ subsystem of the FLEX Triumph™ preclinical PET/CT scanner

N. Zeraatkar
*Department of Radiation Medicine Engineering, Shahid Beheshti University, 1983963113 Tehran, Iran and Research Center for Science and Technology in Medicine, Tehran University of Medical Sciences, 1417613151 Tehran, Iran*

M. R. Ay[a)]
*Research Center for Science and Technology in Medicine, Tehran University of Medical Sciences, 1417613151 Tehran, Iran; Department of Medical Physics and Biomedical Engineering, Tehran University of Medical Sciences, 1417613151 Tehran, Iran; and Research Institute for Nuclear Medicine, Tehran University of Medical Sciences, 1417613151 Tehran, Iran*

A. R. Kamali-Asl
*Department of Radiation Medicine Engineering, Shahid Beheshti University, 1983963113 Tehran, Iran*

H. Zaidi
*Division of Nuclear Medicine and Molecular Imaging, Geneva University Hospital, CH-1211 Geneva, Switzerland and Geneva Neuroscience Center, Geneva University, CH-1205 Geneva, Switzerland*

(Received 17 October 2010; revised 5 January 2011; accepted for publication 6 January 2011; published 11 February 2011)

**Purpose:** X-PET™ is a commercial small animal PET scanner incorporating several innovative designs to achieve improved performance. It is employed as a PET subsystem in the FLEX Triumph™ preclinical PET/CT scanner, the first commercial small animal PET/CT scanner worldwide. The authors report on a novel Monte Carlo (MC) model designed for the evaluation of performance parameters of the X-PET™.

**Methods:** The Geant4 Application for Tomographic Emission (GATE) MC code was used as a simulation tool. The authors implemented more accurate modeling of the geometry of detector blocks and associated electronic chains, including dead-time and time-independent parameters, compared to previously presented MC models of the X-PET™ scanner. Validation of the MC model involved comparison between simulated and measured performance parameters of the X-PET™, including spatial resolution, sensitivity, and noise equivalent count rate (NECR). Thereafter, various simulations were performed to assess scanner performance parameters according to NEMA NU 4-2008 standards with the aim to present a reliable Monte Carlo platform for small animal PET scanner design optimization.

**Results:** The average differences between simulated and measured results were 11.2%, 33.3%, and 9.1% for spatial resolution, sensitivity, and NECR, respectively. The average system absolute sensitivity was 2.7%. Furthermore, the peak true count rate, peak NECR, and scatter fraction were 2050 kcps, 1520 kcps, and 4.7%, respectively, for a mouse phantom and 1017 kcps, 469 kcps, and 18.2%, respectively, for a rat phantom. Spatial resolution was also measured in ten different positions at two axial locations. The radial, tangential, and axial FWHM ranged from 1.31 to 1.96 mm, 1.17 to 2.11 mm, and 1.77 to 2.44 mm, respectively, as the radial position varied from 0 to 25 mm at the centre of the axial field-of-view.

**Conclusions:** The developed MC simulation platform provides a reliable tool for performance evaluation of small animal PET scanners and has the potential to be used in other applications such as detector design optimization, correction of image degrading factors such as randoms, scatter, intercrystal scatter, parallax error, and partial volume effect.  [DOI: 10.1118/1.3547721]

Key words: PET, small animals, Monte Carlo, performance assessment, NEMA standards

## I. INTRODUCTION

The use of small animal models to study human disease in biomedical research has seen a rapid growth during the past two decades. Following the development of the first dedicated rodent PET scanner by the Hammersmith Hospital (London, United Kingdom) in collaboration with CTI PET Systems, Inc. (CTI/Siemens, Knoxville, TN),[1,2] small animal PET systems became very popular and are now playing a big role in many applications requiring the use of molecular imaging techniques to investigate cellular and molecular processes associated with disease in live animals.[3] The FLEX Triumph™ (Gamma Medica-Ideas, Northridge, CA) preclini-

cal PET/CT platform is a dedicated multimodality small animal scanner where the X-PET™ scanner,[4] also known as the Rodent Research PET,[5] was incorporated as the PET subsystem. The latter is a recently designed preclinical PET scanner developed by the *PET Instrumentation Development Group* of the MD Anderson Cancer Center (TX). The main design goals of the X-PET™ were low cost, high-sensitivity, high spatial resolution, and large axial field-of-view (FOV). The use of photomultiplier-quadrant-sharing (PQS),[6] slab-sandwich-slice production technique for building detector blocks more efficiently,[7] in addition to high yield pileup event recovery (HYPER) method,[8] has fulfilled the main goals.[5]

With the widespread availability of different designs of preclinical PET scanners in both academic and corporate settings, the need emerged for adopting a set of protocols and standards for their performance characterization. The results of such standards could provide a proper criterion for comparing different small animal PET systems. The most widely recognized standards are those recommended by the National Electrical Manufacturers Association (NEMA) and one such standard was recently proposed for small animal PET scanners.[9] Since then, some publications reported on the measurement of performance parameters of various preclinical PET systems using this standard.[4,10–17]

Monte Carlo (MC) techniques are widely used for the simulation of medical imaging systems including small animal PET scanners.[18] Up to now, Monte Carlo-based performance assessment of the X-PET™ relied on a rough and simple model of the detector geometry owing to its complexity, which might lead to errors in the obtained results.[19,20] In this work, we sought to develop an accurate MC model of the X-PET™ scanner for use in the evaluation of its performance parameters using the NEMA NU-4 standards and also for further optimization of system design and development and evaluation of image correction techniques. Unlike the simplifications adopted in previously reported MC-based studies of the X-PET™, which overlooked the modeling of the exact geometry of detector blocks and associated electronics, we took the tapered lateral sides of the blocks into account and accurately modeled the electronic structure and features of the X-PET™ scanner. The validity of the model in a variety of simulations was tested against published experimental measurements. The performance of the X-PET™ including sensitivity, count rate characteristics, and spatial resolution was then evaluated based on the NEMA NU-4 2008 standards.[9]

The development of a reliable MC model for the X-PET™ provides several benefits, the most important being that one can rely on simulation results for performance evaluation of the current scanner configuration and for prediction of the achievable performance of novel designs before moving to costly prototyping. Moreover, the model could also be used to investigate and quantify the impact of various physical degrading factors and their correction schemes, including intercrystal scatter, parallax blurring, positron range, noncollinearity of annihilation photons, scatter, and partial volume, or to fully exploit the capacities of iterative reconstruction techniques through accurate modeling of the system matrix.

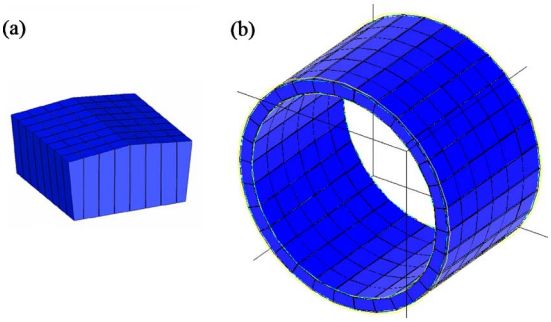


FIG. 1. (a) A sketch of the pentagonal block detector design of the X-PET™. (b) X-PET™ system model implemented in GATE. Every three rows of the blocks consist of a 36° arc containing 18 blocks with one HYPER module covering each of these regions.

## II. MATERIALS AND METHODS

### II.A. PET scanner description

The X-PET™ is a dedicated BGO-based small animal PET scanner incorporating numerous techniques and technological innovations to improve system performance. It applies PQS with a packing fraction of 98% to maximize the sensitivity.[6] In addition, the light guide is absent in this design to increase the light yield of crystals. Moreover, the current design is modified to form circular PQS (CPQS) to improve the system spatial resolution. In the CPQS design, the outer sides of block detectors are ground to decrease the effect of depth of interaction and to ease the optimal arrangement of photomultiplier tubes (PMTs) leading to pentagonal blocks [Fig. 1(a)]. Furthermore, lateral rows of each block are tapered for organizing the blocks in a ring with minimum gap and maximum packing fraction.[5] The most important characteristics and features of the scanner are summarized in Table I.

### II.B. The Monte Carlo model of the X-PET™

In this work, we used the popular Geant4 Application for Tomographic Emission (GATE) MC simulation toolkit owing to its widespread use by the nuclear medicine community.[21] The code is based on well-validated Geant4 libraries[22] to achieve a modular, versatile, scripted simulation toolkit. An important advantage of GATE is that it allows the description of time-dependent observable facts such as source or detector movement and source decay kinetics. This feature provides the possibility to simulate the desired imaging system characteristics under more realistic acquisition conditions.

The first and foremost step in modeling an imaging system in GATE consists in defining its geometry. Geometry definition should be followed by attaching it to a "*System*." The latter is a key concept of GATE providing a template of predefined geometry for simulating a PET scanner.[23] Because of the unconventional geometry of the blocks, a nonstandard model had to be defined as discussed below. This was achieved using *PETscanner* generic system in GATE that gen-

TABLE I. Summary of the X-PET™ features and design parameters.

| Detector | |
|---|---|
| Crystal material | BGO |
| Crystal width (axial) | 2.32 mm |
| Crystal width (transaxial) | 1.36 mm (edge), 2.32 mm |
| No. of crystals per block | 8×8=64 |
| Average crystal depth | 9.4 mm |
| System | |
| No. of detector blocks | 180 |
| No. of crystals | 11 520 |
| No. of detector rings | 48 |
| No. of crystals per detector ring | 240 |
| No. of photomultipliers | 210 |
| Ring diameter | 165 mm |
| Axial FOV | 116 mm |
| Transverse FOV | 100 mm |
| Data set | |
| No. of 3D sinograms | 2304 |
| No. of 2D sinograms | 95 |
| Sinogram size | 255×120 (default) |

erates only ASCII and Root outputs. The inner radius ($R_{min}$) of the PET scanner was set to 82.3 mm.

As mentioned above, our aim was to design a model that takes the pentagonal shape and tapered lateral sides of detector blocks into account in contrast with previous studies that used a cubic model for simplicity.[19,20] We expect the cubic block model to affect the accuracy of results. Therefore, we designed a trapezoidal volume in GATE called "*trpd*" as a model for pentagonal blocks. This geometrical model mimics precisely the real block with respect to tapered lateral sides, although it does not explicitly model the ground outer sides of the block. However, an average depth of 9.4 mm was chosen in the block model to compensate for the ground outer side of the real block. The inner face of the block model is $17.21\times19.12$ mm$^2$, whereas the outer face is $19.23\times19.12$ mm$^2$. The block detector model is monolithic rather than pixelated. Consequently, for image reconstruction purposes, postpixelation was applied to simulate real pixel-based detection.

Accurate calculation of time-dependent performance parameters, such as count rate, calls for a reliable model of PET scanner electronics that is capable of reproducing the behavior of the signal processing chain used on the actual scanner. Data acquisition in the X-PET™ is performed by 10 HYPER modules, each of them handling 18 blocks.[19] For implementing such a structure in our model, we defined a 36° arc of a cylinder with an inner radius equal to that of the PET scanner and repeated the structure for 18 blocks (6 rings with three blocks per ring). Then, this 36° arc was repeated ten times around a ring to compose the whole scanner geometry. Figure 1(b) shows a view of the system model implemented in GATE.

Another important step in the definition of a GATE model is "digitization." In the process of digitization, the electronic response of a detector in a scanner is simulated. This process involves the conversion of the charged particle and photon interactions into energy bins, detection positions, and coincidences. The layout of the X-PET™ digitizer chain is depicted in Fig. 2. Two essential digitizer modules of the chain are the "adder" and "readout." The role of the adder is to translate different hits of a photon or particle to a "pulse," while the readout is associated with the volume in the model whose pulses are acquired as a group.[21,23] For instance, one PMT may be supposed to collect pulses of $8\times8$ crystal elements in a block. With respect to CPQS in X-PET™, the readout is applied on block level in the model. We also defined a "blurring" module with 25% energy resolution at 511 keV that operates on output pulses of the readout module. The "thresholder" module was set to 300 keV for the validation part and 340 keV for the remaining simulations, whereas the "upholder" module was set to 750 keV in all simulations. Furthermore, in order to simulate the effects of dead-time as close to the real system as possible and after consulting with the developers of the X-PET™, two different "dead-time" modules were designed. The first was applied on block level with a value of 350 ns, while the second with a value of 60 ns was implemented on the zones pertaining to HYPER modules. Finally, a "coincidence sorter" with variable timing window was defined for generating coincidence events. We chose a 20 ns window for the initial validation simulations

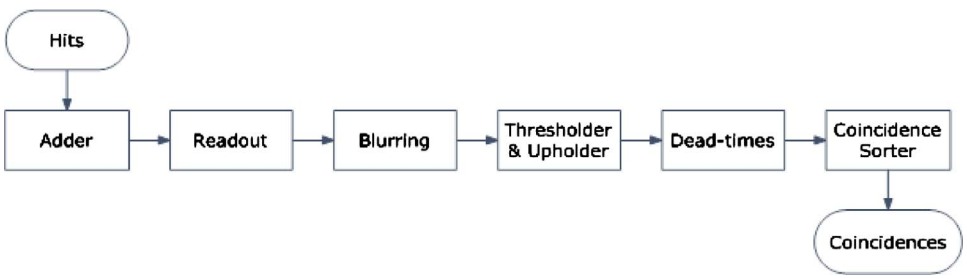


FIG. 2. The layout of the digitizer chain in the GATE Monte Carlo model representing the X-PET™ scanner. The adder is the first module of the digitizer chain in charge of summing all the hits that occur within the same crystal. The readout module sums the pulses of the adder modules that are inside its corresponding volume. The blurring module emulates Gaussian blurring of the corresponding energy of a pulse after the readout module. The thresholder and upholder modules consider the effect of the energy window. The dead-time module is applied on appropriate volumes in the MC model to simulate the impact of dead-time in the real detection system. Finally, the coincidence sorter module generates coincidence events according to the predefined time window.

and a 16 ns window for the performance simulations based on NEMA specifications.

### II.C. Validation

The developed MC model was validated by performing three sets of simulations measuring sensitivity, noise equivalent count rate (NECR), and spatial resolution according to the experimental setup described in Ref. 20. We then compared our results to those reported in that work.

#### *II.C.1. Spatial resolution*

In the work of Baghaei *et al.*,[20] experimental measurements of spatial resolution were performed using a 0.25 mm diameter spherical Na-22 source surrounded by a 2 mm thick aluminum (Al) wall, utilized for assessment of spatial resolution. The point source was scanned at five positions with different radial displacements while axially centered. In the simulation study, the same source and above described setup were adopted. An activity of 200 kBq was used with an acquisition time of 60 s for each position. The collected three-dimensional (3D) data were then rebinned into 95 two-dimensional (2D) sinograms using single-slice rebinning[24] (SSRB) considering a maximum ring difference (MRD) of 20. Then, transverse images were reconstructed using 2D ordered subsets-expectation maximization (OSEM) algorithm with 15 subsets and 4 iterations.

#### *II.C.2. Sensitivity*

The same source used for spatial resolution measurement was used in experimental measurements of sensitivity.[20] The point source was centered in the scanner's field-of-view both axially and transaxially. Similarly, in the simulation, we modeled the same Na-22 source and Al wall at the center.

#### *II.C.3. NECR*

A 12 cm long cylindrical rat-sized phantom with inner and outer diameter of 4 and 5 cm, respectively, was used in Ref. 20 for experimental measurement of count rate performance. We implemented the same phantom for simulation. However, while a phantom filled with F-18 solution is used in the experimental setup, we applied 511 keV back-to-back annihilation photons in our simulations to decrease computation time. The simulations were performed using five different values of uniformly distributed activity. The NECR was defined as

$$\mathrm{NECR} = T^2/(T+S+R), \tag{1}$$

where $T$, $S$, and $R$ are the true, scatter, and random coincidence rates, respectively.

### II.D. Performance assessment using the NEMA NU-4 2008 standards

Following the above validation, performance parameters of the X-PET™ scanner were evaluated according to NEMA NU-4 2008 protocols using the validated MC model. Simulations based on the NEMA specifications were performed to estimate spatial resolution, sensitivity, and count rate performance.

#### *II.D.1. Spatial resolution*

A spherical Na-22 source (0.3 mm in diameter) of activity 200 kBq, surrounded in an acrylic cube (10 mm in all sides), was scanned in two axial positions: At the center of the axial FOV and at one-fourth of the axial FOV (28.95 mm from the center along the axial direction) and five radial positions (0, 5, 10, 15, and 25 mm radial distances from the center) for each of the two axial positions. Data acquisition time was set to collect at least 100 000 prompt counts for each position. Thereafter, the acquired 3D data were rebinned into 2D sinograms using Fourier rebinning (FORE) and a MRD of 20. Finally, image reconstruction was performed using 2D filtered backprojection (FBP) with maximum cutoff frequency and no axial filtering.

#### *II.D.2. Sensitivity*

Following the NEMA NU-4 2008 protocol, a spherical Na-22 source (0.3 mm in diameter) embedded in an acrylic cube (10 mm in all sides) was used for measurement of sensitivity. A 200 kBq point source ($A_{\mathrm{cal}}$) was used which satisfied the NU-4 recommendations on count losses and random rate. In the first step, the source was placed at the center of the scanner both axially and transaxially and 10 000 true counts were collected. The time required was determined as $T_{\mathrm{acq}}$. The source was then stepped axially to both sides of the scanner with a step size corresponding to slice thickness (1.22 mm). In each step, the data were collected for the same acquisition time ($T_{\mathrm{acq}}$). After each acquisition, SSRB was applied to the 3D PET data to generate 95 2D sinograms. In each sinogram, the pixel having the largest value in each row (angle) was determined and all pixels located 1 cm from this pixel were set to zero. No correction for scatter, random counts, or decay was applied. Finally, all pixels were summed to calculate the total counts in each plane. By dividing the total counts by $T_{\mathrm{acq}}$, the count rate ($R_i$) for each plane in counts per second was determined.

According to NEMA NU-4, the sensitivity (in counts/Bq s) and the absolute sensitivity, obtained by taking the branching ratio of Na-22 into account, were calculated for each plane using Eqs. (2) and (3), respectively.

$$S_i = \left(\frac{R_i - R_{B,i}}{A_{\mathrm{cal}}}\right), \tag{2}$$

$$S_{A,i} = \frac{S_i}{0.906} \times 100, \tag{3}$$

where the index $i$ indicates the plane number and $S$, $S_A$, $R$, $R_B$, and $A_{\mathrm{cal}}$ represent sensitivity, absolute sensitivity, count rate, background count rate (not present in simulation), and source activity, respectively.

### *II.D.3. Count rate performance and scatter fraction*

Depending on the scanner's size, NEMA NU-2 2008 recommends to measure count rate performance using any or a combination of three phantoms (mouselike, ratlike, and monkeylike), which are structurally similar but have different sizes. For the X-PET™ scanner, both the mouselike and ratlike phantoms were used in our study.

The mouse phantom consists of a solid, high density polyethylene ($\rho$=0.96 g/cm$^3$) cylinder 25 mm in diameter and 70 mm high. A cylindrical hole (3.2 mm diameter) is drilled parallel to the central axis at a radial distance of 10 mm, the central part of which (60 mm length) is used for inserting a uniformly distributed line source. The rat phantom is larger, having a diameter of 50 mm and a height of 150 mm, where the same cylindrical hole is located at a radial distance of 17.5 mm with the central part covering 140 mm. Both phantoms are composed of high density polyethylene ($\rho$ =0.96 g/cm$^3$). The properties of both phantoms were used as input in the simulation study. We simulated F-18 as the radionuclide (with modeling of positron range and photon noncollinearity) and used varying initial activity for each acquisition. Each acquisition should be long enough to collect at least 500 000 prompt counts, while it should be shorter than one-fourth the radionuclide's half-life. In addition, acquisitions should be frequent enough to cover peaks of true and NEC rates and be continued until the random event rate is small enough. Following rebinning, the sinograms were processed according to NEMA standards to calculate total, true, random, and scatter events rate.

Using count rates of low activity acquisitions, a measurement of the coincidence count rate free from random coincidences was obtained. By extrapolating the true rate to higher activity levels and comparing it to the registered rate, count losses at higher activity levels were estimated for both the mouse and rat phantoms.

The scatter fraction (SF) of the system for both phantoms was calculated using the following equation:[9]

$$\mathrm{SF} = \frac{\Sigma_i \Sigma_{j'} C_{r+s,i,j'}}{\Sigma_i \Sigma_{j'} C_{TOT,i,j'}}, \tag{4}$$

where $C_{r+s,i,j'}$ and $C_{\mathrm{TOT},i,j'}$ represent the sum of random and scatter and total counts, respectively, in the $i$th plane during the $j$th acquisition, in which count loss and random rates are low enough.

## III. RESULTS

### III.A. Validation study

Figure 3 compares simulated and measured radial and tangential spatial resolution versus radial offset. For each position of the point source, the reconstructed image of the central slice was used to calculate the full width at half maximum (FWHM) of the point spread function in both radial and tangential directions. To this end, the one-dimensional (1D) radial and tangential profiles were independently fitted with a Gaussian curve to derive the FWHM. Despite small discrepancies at the center and most extreme radial position for the radial spatial resolution, it can be seen that simulation results follow the same trend and are in agreement with experimental measurements, especially for the tangential spatial resolution where the relative difference is close to 6%.

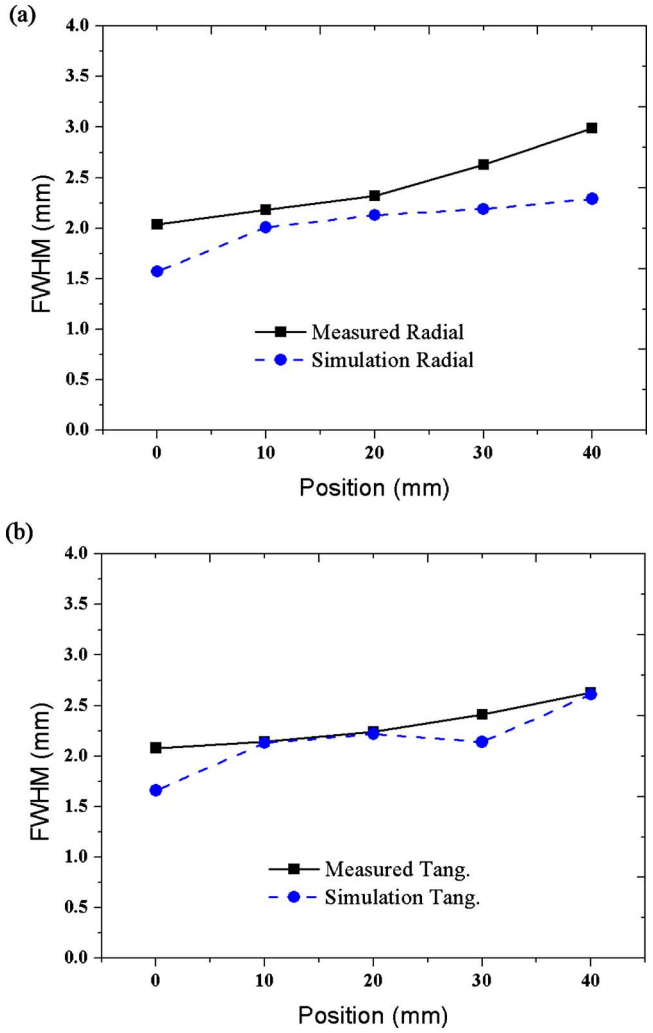


FIG. 3. Comparison between simulated and measured (a) radial and (b) tangential spatial resolution of the X-PET™ scanner.

The absolute sensitivity was calculated as the ratio of total coincidence rate to the point source activity. While experimental measurement reports a sensitivity of 8.4%,[20] our simulation resulted in sensitivity of 11.2% for the X-PET™ scanner. The reason for this discrepancy is that light transport was neglected in our MC simulations leading to the approximation that the whole energy of each detected event by the crystal was perfectly converted to an electrical pulse, i.e., an efficiency of 100% for conversion of energy deposited in the crystal into electrical pulses. The overestimation of the sensitivity is compensated by a scaling mechanism to enable a more accurate estimation of the NECR.

Figure 4 compares simulated and measured NECR curves for a uniformly distributed activity concentration in the rat-sized phantom. A global scaling factor was defined to compensate for the difference between simulated and experimen-

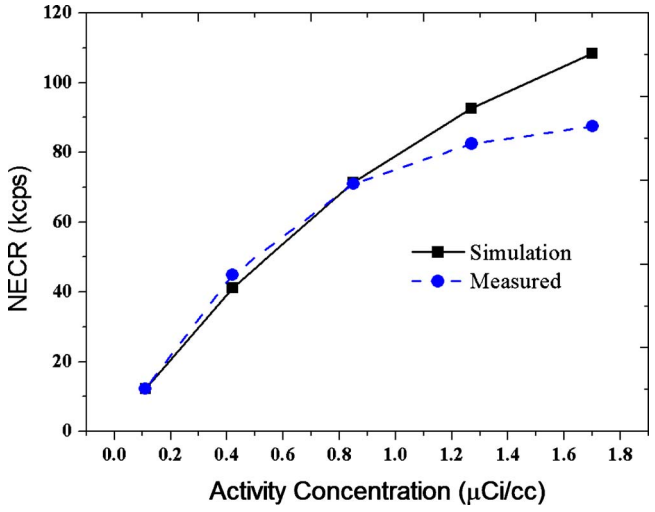


FIG. 4. Comparison between simulated and measured NECR estimates of the X-PET™ for a rat-sized phantom. Simulation data were normalized to match the experimental results for sensitivity in the lowest activity range.

tally measured sensitivity at low count rate.[20] The scaling factor was calculated as the ratio of the measured NECR to the simulated NECR at the lowest activity. All the simulated values of NECR were then multiplied by the scaling factor. As can be seen in Fig. 4, simulated values of the NECR are in good agreement with experimental results, particularly for low activity concentrations. The average difference between the simulated and measured values of NECR at various activity concentrations was 9.1%. The complicated combination of dead-time effects of different hardware components of the system, particularly at higher activity levels, causes the differences between experimental and simulated results to increase at higher activity concentration.

### III.B. Performance assessment using NEMA NU-4 2008 standards

The spatial resolution in terms of FWHM and FWTM of the point spread function was determined through the peak of the image volume in the three orthogonal directions. The point spread function was formed by summing all 1D profiles parallel to the direction of measurement. The FWHM and FWTM were determined by linear interpolation between adjacent pixels at half and tenth maximum value of the response function, respectively. The maximum value was determined by a parabolic fit using the peak point and its two nearest neighbors. Figure 5(a) shows the radial, tangential, and axial spatial resolution for different point source locations. Figure 5(b) shows the volumetric resolution computed by multiplying the FWHM in the radial, tangential, and axial direction. The difference between the results reported in the validation step and NEMA assessments can be explained by the difference between rebinning (SSRB was used for validation, whereas FORE was employed for NEMA) reconstruction algorithms used (OSEM was used for validation whereas FBP was employed for NEMA). In addition, the method used for calculating the FWHM was different

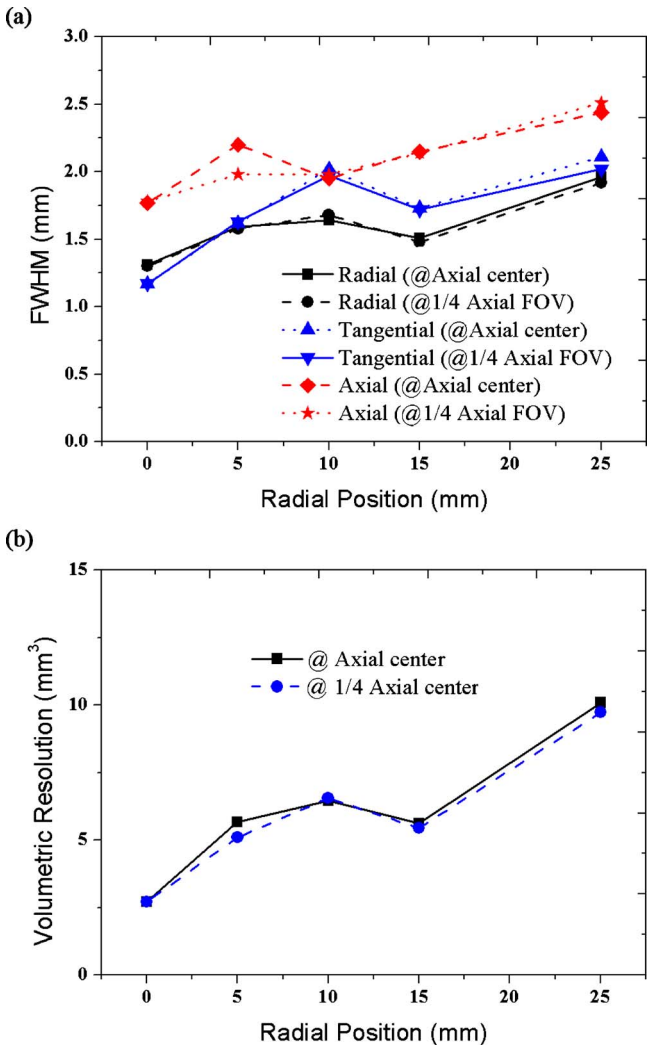


FIG. 5. (a) Simulated spatial resolution of the X-PET™ scanner in terms of FWHM according to NEMA NU-4 standards. (b) Resulting volumetric spatial resolution obtained by multiplication of radial, tangential, and axial FWHMs.

(Gaussian fit of 1D profile was used for validation, whereas NEMA calculations were done without fitting).

The absolute sensitivity profile versus axial position is depicted in Fig. 6(a). Since the data are acquired in 3D mode, as the position of the source gets closer to the center of the axial FOV, the slice sensitivity increases and, consequently, the sensitivity profile reaches its peak (42 cps/kBq) at the central slice. Furthermore, the sensitivity of one-half of the axial planes was fitted with a linear function, showing the sensitivity homogeneity of the scanner. The corresponding result is illustrated in Fig. 6(b) showing a good correlation coefficient ($R^2$=0.977) for the fitted line. A summary of sensitivity-related parameters as defined in the NEMA NU-4 2008 standard is reported in Table II. It should be emphasized that $SR_{tot}$ and $S_{tot}$ (and, similarly, $SR_{A,tot}$ and $S_{A,tot}$) are equal because the axial extent of the rat phantom (15 cm) is larger than the axial FOV of the scanner and, as such, all slices are considered for the calculation of these parameters.

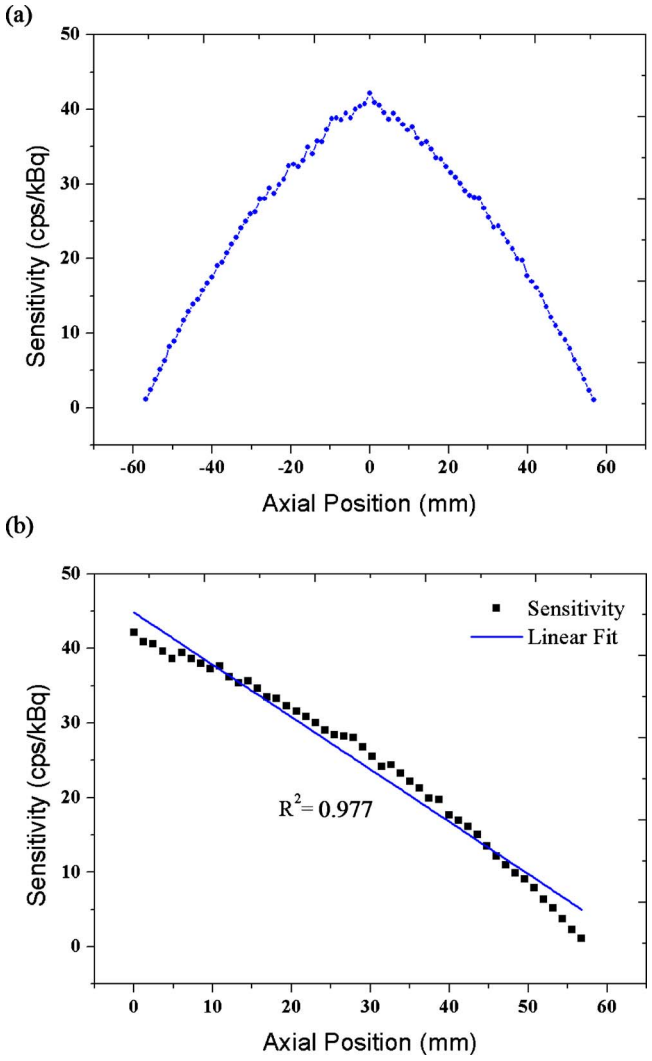


FIG. 6. (a) Sensitivity profile of the X-PET™ scanner over axial positions calculated according to NEMA NU-4 2008 standards. (b) Homogeneity of the sensitivity profile along the axial direction.

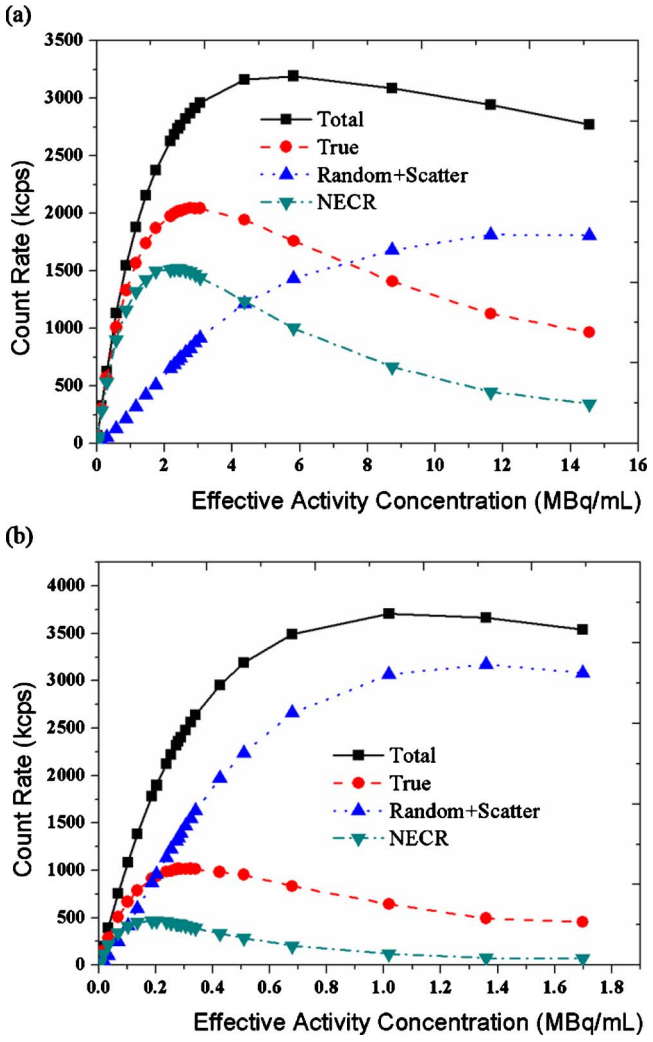


FIG. 7. Count rate curves versus average effective activity concentration measured according to NEMA NU-4 2008 standards for (a) mouse-sized and (b) rat-sized phantoms.

To calculate count rate performance, 32 acquisitions were simulated for the mouse phantom and 34 acquisitions for the rat phantom starting from an initial activity of 500 down to 10 kBq. An adequate number of counts was acquired for each acquisition. Our results show that the peak true count rate for the mouse and rat phantoms was 2050 (at 2.765 MBq/ml) and 1017 kcps (at 0.280 MBq/ml), respectively. In addition, the peak NECR for the mouse and rat phantom was 1520 (at 2.401 MBq/ml) and 469 kcps (at 0.187 MBq/ml), respectively. The system true event rate, sum of random and scatter event rate, total event rate, and NECR for the mouse and rat phantoms are plotted against the average effective activity concentration in Fig. 7. The system count loss was 25% at 0.646 MBq/ml and 50% at 1.621 MBq/ml for the mouse phantom, whereas it was 25% at 0.074 MBq/ml and 50% at 0.188 MBq/ml for the rat phantom. Finally, the system SF for the mouse and rat phantoms was calculated as 4.7% and 18.2%, respectively.

TABLE II. Sensitivity parameters of the X-PET™ scanner based on NEMA NU-4 standards.

| | |
|---|---|
| Average system sensitivity for mouse phantom ($SM_{tot}$) | 33 cps/kBq |
| Average system sensitivity for rat phantom ($SR_{tot}$) | 25 cps/kBq |
| Average absolute system sensitivity for mouse phantom ($SM_{A,tot}$) | 3.7% |
| Average absolute system sensitivity for rat phantom ($SR_{A,tot}$) | 2.7% |
| Average total system sensitivity ($S_{tot}$) | 25 cps/kBq |
| Average total absolute system sensitivity ($S_{A,tot}$) | 2.7% |

## IV. DISCUSSION

A validated MC model of a PET scanner provides a suitable platform for performance evaluation of the scanner or for prediction of the achievable performance of improved/optimized versions or novel designs. Alternatively, it is a useful tool for assessment of the effect of physical degrading factors and their correction or incorporation in statistical image reconstruction techniques. The developed MC model of

the X-PET™ scanner fulfills both criteria and constitutes the first step to reach our endeavors.

Model validation involved carrying out simulation studies replicating the experimental setups reported in previously published reports for the same scanner.[20] Figure 3 demonstrates good agreement between MC simulated and experimentally measured spatial resolution in radial and tangential directions. The lack of accurate modeling of intercrystal light cross talk could have a significant role in the deviation between MC and measured results, particularly at large radial offsets for the radial spatial resolution. Another explanation is the assumption of perfect position decoding of the events in the simulation study.

The assessment of spatial resolution showed that the FWHM in radial, tangential, and axial directions remained below 1.96 mm. The degradation of spatial resolution in the radial and axial directions is mostly due to the increase in the proportion of coincidences subject to parallax errors as the radial offset gets larger. However, the tangential resolution remained almost constant when increasing the radial offset. Overall, the spatial resolution of the X-PET™ scanner is slightly lower but of the same order as other high-resolution small animal PET scanners.[10,13,15] Higher and more uniform spatial resolution could be obtained by using fully 3D statistical iterative reconstruction algorithms incorporating accurate modeling of PET scanner response.[25]

The overestimation of the sensitivity by the MC model (11.2%) in comparison with experimental measurements (8.4%) is expected since light transport and PMT efficiency are not modeled in GATE. However, this discrepancy will not affect other simulated performance parameters since this was compensated for using the aforementioned scaling process. The spatial resolution is independent of the sensitivity; the latter might instead alter the signal-to-noise ratio. The MC calculated NECR in a typical rat phantom is in good agreement with the measured results following scaling of the obtained results as reported by Baghaei *et al.*[20] The small deviations at high activity levels are due to the weaknesses of the GATE MC toolkit in simulating the complicated behavior of system dead-time at high activity levels (Fig. 7).

Following the validation study, three sets of simulation studies were performed to evaluate performance parameters of the X-PET™ scanner using the NEMA NU-4 2008 standards. Figure 6(a) shows that when applying SSRB on 3D PET data using a MRD of 47, the system sensitivity peak reaches 42 cps/kBq at the center of the axial FOV and decreases as the axial distance from the center increases. This trend is understandable given the decrease of the acceptance angle of the detection system with the increase of axial distance from the center. Furthermore, Fig. 6(b) demonstrates the homogeneous behavior of the sensitivity along the axial direction. The average absolute system sensitivity for mouse-sized and rat-sized phantoms is 3.7% and 2.7%, respectively, which is comparable to estimates reported for the Inveon™ PET scanner (4.0% and 2.8% for the same mouse and rat phantoms, respectively).[13] It should be noted that PET data were acquired using an energy window of 340–750 keV and a time window of 16 ns for the X-PET™, whereas they were acquired using an energy window of [250–625] keV and a time window of 3.43 ns for the Inveon™ PET scanner.

Figure 7 shows the count rate behavior in mouse and rat phantoms as a function of activity concentration. The peak NECR for mouse and rat phantoms is 1520 and 496 kcps, respectively, which is lower but still comparable to values reported for the Inveon™ PET scanner (peak NECR of 1670 and 590 kcps for mouse and rat phantoms, respectively).[13] The smaller NECR in the rat phantom results from the larger amount of scattering medium and, consequently, the larger path annihilation photons have to travel to reach the detectors, which in turn increases the probability of Compton scattering and attenuation of true coincidences. The SF for mouse-sized and rat-sized phantoms was 4.7% and 18.2%, respectively, compared to 7.8% and 17.2% for the Inveon™ PET scanner.[13] Larger values were reported for both phantoms (11.45% and 23.26%) for the VrPET scanner.[10]

## V. CONCLUSION

An accurate MC model was developed for the X-PET™, the PET subsystem of the FLEX Triumph™ preclinical PET/CT scanner. The MC model was validated through comparison with experimental measurements under similar conditions. This allowed the assessment of performance parameters of the system using the NEMA NU-4 2008 standards. The results show that the X-PET™ can be considered as a high-sensitivity and high-resolution preclinical PET scanner. Our ultimate goal is to use the model to investigate and quantify the impact of various physical degrading factors and their correction schemes, including intercrystal scatter, parallax errors, positron range, noncollinearity of annihilation photons, scatter, and partial volume effect, and to exploit the capacities of iterative reconstruction techniques through accurate modeling of the PET acquisition process for derivation of the system matrix to reach an improved and uniform spatial resolution across the whole FOV.

## ACKNOWLEDGMENTS

This work was supported by the Research Center for Science and Technology in Medicine and Tehran University of Medical Sciences, Tehran, Iran under Grant No. 10479 and the Swiss National Science Foundation under Grant No. 31003A-125246. The authors would like to thank Dr. H. Baghaei and Dr. Y. Zhang from the MD Anderson Cancer Center for valuable discussions.

[a]Author to whom correspondence should be addressed. Electronic mail: mohammadreza_ay@tums.ac.ir; Telephone: +0098 21 64053255; Fax: +0098 21 66466383.

[1]S. Rajeswaran *et al.*, "Dynamic monitoring of [11C]diprenorphine in rat brain using a prototype positron imaging device," J. Neurosci. Methods **40**(2–3), 223–232 (1991).

[2]P. M. Bloomfield *et al.*, "The design and physical characteristics of a small animal positron emission tomograph," Phys. Med. Biol. **40**(6), 1105–1126 (1995).

[3]C. S. Levin and H. Zaidi, "Current trends in preclinical PET system design," PET Clinics **2**(2), 125–160 (2007).

[4]R. Prasad, O. Ratib, and H. Zaidi, "Performance evaluation of the FLEX triumph X-PET scanner using the national electrical manufacturers association NU-4 standards," J. Nucl. Med. **51**(10), 1608–1615 (2010).

[5]W. H. Wong *et al.*, "Design of an inexpensive high-sensitivity rodent-research PET camera (RRPET)," in the 2003 IEEE Nuclear Science Symposium Conference Record, Vols. 1–5, pp. 2058–2062, 2004.
[6]W. H. Wong, "A positron camera detector design with cross-coupled scintillators and quadrant sharing photomultipliers," IEEE Trans. Nucl. Sci. **40**(4), 962–966 (1993).
[7]J. Uribe *et al.*, "An efficient detector production method for position-sensitive scintillation detector arrays with 98% detector packing fraction," IEEE Trans. Nucl. Sci. **50**(5), 1469–1476 (2003).
[8]H. Li *et al.*, "A new pileup-prevention front-end electronic design for high-resolution PET and gamma cameras," IEEE Trans. Nucl. Sci. **49**(5), 2051–2056 (2002).
[9]National Electrical Manufacturers Association, NEMA Standards Publication NU 4-2008 (Performance Measurements of Small Animal Positron Emission Tomographs, 2008).
[10]E. Lage *et al.*, "Design and performance evaluation of a coplanar multimodality scanner for rodent imaging," Phys. Med. Biol. **54**(18), 5427–5441 (2009).
[11]W. Luo, E. Anashkin, and C. G. Matthews, "First test results of a commercially available clinical PET scanner using the NEMA NU 4–2008 small animal PET standards," in the IEEE Nuclear Science Symposium Conference Record, pp. 4718–4723, 2008.
[12]M. Canadas *et al.*, "Performance comparison of two commercial small animal PET scanners: ClearPETT and rPET-1T," in the IEEE Nuclear Science Symposium Conference Record, pp. 4773–4779, 2008.
[13]Q. Bao *et al.*, "Performance evaluation of the Inveon dedicated PET preclinical tomograph based on the NEMA NU-4 standards," J. Nucl. Med. **50**(3), 401–408 (2009).
[14]E. Lage *et al.*, "VrPET/CT: Development of a rotating multimodality scanner for small-animal imaging," in the IEEE Nuclear Science Symposium Conference Record, pp. 4671–4674, 2008.
[15]S. A. Kis *et al.*, "Performance test of the MiniPET-II small animal scanner according to the NEMA NU-4 standard," in the IEEE Nuclear Science Symposium Conference Record, pp. 3185–3189, 2009.
[16]F. D. Popota *et al.*, "Comparison of NEMA NU 4–2008 vs NEMA NU 2–2001 for the performance evaluation of the microPET R4 system," presented at the IEEE Nuclear Science Symposium Conference Record, pp. 1082–3654, 2009.
[17]W. Luo, E. Anashkin, and C. G. Matthews, "Performance evaluation of a PEM scanner using the NEMA NU 4—2008 small animal PET standards," IEEE Trans. Nucl. Sci. **57**(1), 94–103 (2010).
[18]H. Zaidi, "Relevance of accurate Monte Carlo modeling in nuclear medical imaging," Med. Phys. **26**(4), 574–608 (1999).
[19]Y. X. Zhang *et al.*, "Performance evaluation of the low-cost high-sensitivity rodent research PET (RRPET) camera using Monte Carlo simulations," in the IEEE Nuclear Science Symposium Conference Record, Vols. 1–5, pp. 2514–2518, 2005.
[20]H. Baghaei *et al.*, "GATE Monte Carlo simulation of a high-sensitivity and high-resolution LSO-based small animal PET camera," IEEE Trans. Nucl. Sci. **54**(5), 1568–1573 (2007).
[21]S. Jan *et al.*, "GATE: A simulation toolkit for PET and SPECT," Phys. Med. Biol. **49**(19), 4543–4561 (2004).
[22]S. Agostinelli *et al.*, "GEANT4: A simulation toolkit," Nucl. Instrum. Methods Phys. Res. A **506**, 250–303 (2003).
[23]S. Jan *et al.*, GATE users' guide, v4.0.0, OpenGATE Collaboration, 2008.
[24]M. E. Daube-Witherspoon and G. Muehllehner, "Treatment of axial data in three-dimensional PET," J. Nucl. Med. **28**(11), 1717–1724 (1987).
[25]M. S. Tohme and J. Qi, "Iterative image reconstruction for positron emission tomography based on a detector response function estimated from point source measurements," Phys. Med. Biol. **54**(12), 3709–3725 (2009).